Alternative Reinforcement Products in the Design of Concrete Structures — Durability Performance

Marti Hudecek, Bridge Engineer, Stantec Consulting Ltd.

Kip Skabar, BC Transportation Practice Leader, Stantec Consulting Ltd.

Raafat El-Hacha, Professor of Structural Engineering, University of Calgary

Paper prepared for presentation at the STRUCTURES Session

at the 2020 TAC Conference & Exhibition

Acknowledgements:

For generous donation of the rebars, we would like to thank to: Harris Rebar, MMFX Technologies-a CMC company, V-rod Canada, Hughes Brothers Inc., and Shanghai Shen Xiang CO, Ltd. We appreciate the work of Mauhammad Amiry, a Master of Science student, who carried out the laboratory work at the University. We would like to thank to Oba Harding, representing Mitacs at the University, for his help to facilitate the financial support via grand Accelerate. We acknowledge also Natural Sciences and Engineering Research Council of Canada (NSERC) for their financial support via grand Engage.

ABSTRACT

The presented work focuses on performance evaluation of concrete beams reinforced in flexure with seven different types of rebars. This research takes a holistic approach and is intended to assist engineers, designers, and asset owners with making informed decisions when selecting appropriate reinforcement in a variety of concrete structure applications.

Selection of a suitable type of a corrosion resistant rebar is a complex process and depends on not only initial cost and maintenance but also the overall performance of the structural member. While research examining individual types of advanced reinforcing materials have been conducted in the past, rigorous evaluations of multiple different types of materials tested simultaneously under comparable conditions are rare. Therefore, this research investigated the durability performance of concrete beams reinforced with different types of internal flexural rebars, metal-based and non-metal-based materials, including Fibre Reinforced Polymer (Basalt, Carbon and Glass), Martensitic Micro-Composite Formable Steel, and stainless steel, in addition to the conventional uncoated black steel for comparison purposes. The test specimens represented a bridge parapet and were exposed to identical harsh environmental conditions in a state-of-the-art climate chamber that simulated extended periods of exposure.

In total, twenty-eight reinforced concrete beams were tested for ultimate flexural capacity. All beams were pre-cracked until reaching service conditions and kept loaded with a sustained load of 40% of their ultimate carrying capacity. Twenty-one beams were subjected to severe environmental conditions and subjected to 195 accelerated freeze-thaw cycles (equivalent to five years of real-life exposure) over a period of two months combined with spraying with a 3.5% sodium chloride (NaCl) rich water solutions representing accelerated exposure to traffic spray zones. The duration of each cycle was eight hours with temperature varying from -34°C to +34°C with a relative humidity of 75% for temperatures above +20°C. The remaining seven beams were kept at normal ambient temperature of 22-24°C and served as control specimens for comparison purposes.

The beams were designed to develop similar flexural capacity and their structural performance is described in detail considering the different nature of the reinforcing materials. The following categories were evaluated: cracking patterns at service loads, cracking patterns at ultimate loads, ultimate flexural capacity and failure modes, corrosion resistance of the rebars, load-deflection behaviour, and ductility. A summary matrix table was developed as a guideline to serve in a selection-making process as each reinforcing material offers different advantages that may be suitable for specific conditions.

1 INTRODUCTION & MOTIVATION

Resiliency and durability of structures are attributes oftentimes applied among engineers, designers, planners, asset manager, and owners. In reinforced concrete structures, it is the internal reinforcement that plays the key role. Internal reinforcement does not affect only the initial cost, constructability, and strength of structural members, it foremostly influences long-term cost and maintenance relevant expenditures, lifespan, as well as performance of the surrounding concrete. It can be said that internal reinforcement affects all stages of a structure's life influencing its performance and contributing to its safe use. Therefore, it is crucial to give a proper attention to select suitable material for given application.

The key issue of internal reinforcement is its susceptibility to corrosion. In civil engineering applications uncoated mild steel, aka, black steel, has been widely used. This material has gained great popularity over the years for its low initial cost, ductile behavior it reinforces, and ease of recycle and reuse. However, in applications such as bridges, parking garages and/or marine terminals, the elevated presence of chloride-rich solutions causes the black bar to corrode, and therefore, weakens its performance and increases the rate of deterioration of the concrete. This effect is yet magnified by contribution of weather conditions, significantly affected by ongoing climate change.

Since the turn of the century, significant efforts across industry have been put into research focusing on corrosion resistant applications. A number of advanced materials have been developed, tested, and applied in projects. While extensive research has been done and it is still ongoing, typically, only a narrow group of materials is evaluated at one time. Therefore, in our research, seven different materials have been selected, exposed to identical climate conditions, and evaluated following the same protocol to establish a reliable reference assuring optimal material use and safe operation of the structure.

2 OBJECTIVES

In our research, we selected seven different types of bars to internally reinforce concrete beams representing a bridge parapet exposed to service and ultimate loads under the influence of harsh weather conditions combined with chloride rich water solutions. The two main goals were to evaluate the effect of the environmental exposure on durability performance of beams and to establish a guideline that could be used in a process of selecting a suitable type of a corrosion resistant reinforcement in applications governed by flexural loads. To achieve our goals, we established several categories at which the beams' performance was evaluated. The categories were: cracking patterns at service loads, cracking patterns at ultimate loads, failure modes and flexural capacity, load-deflection relationship, and ductility.

3 RESEARCH CARRIED OUT TO DATE

To date, many different research initiatives have been carried out to search for feasible solutions to corrosion of black bars in concrete structures. Not all the achievements have significant impact for extended periods of time. Products such as epoxy coated steel gained popularity due to extended durability and relatively low cost, in comparison to advanced composite materials. Nevertheless, the quality of the coating and its susceptibility to damage during installation creates a challenge. Many

provincial jurisdictions no longer recommend such products as per Shao et al. (2009) and Kahl (2007). Migrating corrosion inhibitors (MCI) represent a cost-effective solution; however, tend to be less effective in harsh environments, Ormelese et al. (2007). Applications such as cathodic protection are effective; however, require additional effort during installation and last only for limited amount of time, Polder et al. (2014). Hence, applications simplifying the installation and extending the life of the assembly thanks to the internal reinforcing bar itself were sought.

Considering the material characteristics, there are two groups of reinforcing bars: metal-based and non-metal-based bars. Fibre Reinforced Polymers (FRP) represent the non-metal-based rebar. These materials do not corrode. The main differentiating attribute of these bars is "linear behavior" up until failure; FRP bars do not experience yielding plateau, which is typical for metal-based bars. FRPs utilize properties of corrosion resistant high-strength fibers of different kinds such as glass (GFRP), carbon (CFRP), basalt (BFRP), and aramid (AFRP). Artificial resins, for example vinylester, polyesters, epoxy, or silicones, serve as a binding matrix surrounding and protecting the fibres. These materials are typically attributed with high strength-to-weight ratio and outstanding durability. Some FRPs exhibit relatively low modulus of elasticity (E), resulting in large deformations, Micelli et al. (2004). The loss of bond strength between the FRP rebar and concrete may occur when exposed to severe environmental conditions, Chen et al. (2007)].

Stainless steel and Martensitic Micro-composite Formable Steel (MMFX) represent durable metal-based materials. In Canada, stainless steel is commonly used as a top layer of reinforcement in decks and barriers for its corrosion resistance and mechanical properties similar in nature to conventional black bar. MMFX, while being an example of corrosion resistant metal-based bars, slightly differs from conventional black bar-mainly due to its chemical composition. This material is supplied in several grades based on selected level of chromium. MMFX bars typically experience higher yield and ultimate tensile strength relative to black bars, which may be beneficial in specific applications and less beneficial in others.

Properties of advanced materials have been tested by number of researchers. For example, Micelli et al. (2004) investigated the effect of severe environmental conditions at accelerated rate including cycles of freezing and thawing, exposure to high humidity and temperature, and exposure to ultraviolet (UV) rays on the long-term durability of GFRP and CFRP bars. Durability of GFRP rebar embedded in the concrete was studied by Chen et al. (2007). Bond strength of GFRP and CFRP rebar, influenced by exposure to water and elevated temperatures, was tested by Davalos et al. (2008). Durability of newly emerging BFRP was investigated by Quagliarini et al. (2016) and Lu et al (2015). Fatigue performance of MMFX rebar in corrosive environment, i.e., coupling the effect of cyclic loading and corrosion, studied by DeJong et al. (2009), showed a significant improvement in the durability of this material in comparison to conventional black bar. The corrosion resistance is typically four to eight time higher than in black bar, Kahl (2007).

4 SIGNIFICANCE OF ENVIRONMENTAL EXPOSURE

The significance of climate change is being reflected in a wide range of industrial projects, in road and bridge designs especially. To simulate environmental conditions correctly, parameters such as temperature, relative humidity, location, number of applied exposure cycles, and presence of other chemicals-for example as deicing salts-need to be derived carefully.

From the wide range of entry parameters, the number of cycles plays a significant role. Most researchers have considered 300 freeze-thaw cycles. As can be found in the literature, the selected number of cycles by the researchers is arbitrary and depends on the location of the structure and many environmental factors making it difficult to estimate for the corresponding lifetime. Nevertheless, it is believed that the nature of the simulated cycles in climate chambers used to accelerate the exposure is more severe than what would be typically encountered in reality, and it is possible to have an estimation of the minimum corresponding lifetime having the annual freeze-thaw frequency of the relevant geographic location.

For a city such as Toronto, which has about 33 to 39 freeze-thaw cycles per year, Ho and Gough (2005) estimated 650 cycles occur over 16 to 20 years. However, the accelerated exposure makes it much more severe (three cycles a day) than real life freeze-thaw cycles. Bisby and Green (2002) estimated that 300 freeze-thaw cycles with lower and upper temperatures of -18˚C and +18˚C, respectively, at a rate of one cycle per day (16 hr at -18 ˚C, thawing in a water bath for 8 hrs), was equivalent to somewhere between 10 to 20 years for an exterior exposure application in Toronto. Laoubi et al. (2006) estimated that freeze-thaw cycles ranging from 100 to 360, with one cycle every 12 hr (6 hr to -20˚C and 6 hr to 20˚C) and Humidity of 50% during all freeze-thaw exposure, conservatively covers the lifetime of a structure in North America.

Therefore, considering an average freeze-thaw frequency of 39 cycles per year for Canada, Fraser (1959), the accelerated 500 cycles used in the study by Omran (2013) (500×8 hr = 4000 hr = 166.7 day), that is equivalent to 0.457 year of exposure inside the chamber, corresponds to a minimum lifetime of 12.8 years. This exposure regime was adopted in the research by Omran and El-Hacha (2014) in which 500 freeze-thaw cycles were applied to investigate the effects of long-term severe exposure and high number of the cycles on the performance of RC beams strengthened with prestressed FRP strips and bars. Omran and El-Hacha (2014) reported that spraying fresh water directly on the beam at a rate of 18 Liters per minute is more severe than maintaining a humidity level of 75%, which is the annual average relative humidity in Canada, inside the environmental chamber. This estimation clearly shows that the exposure regime adopted by Rojob and El-Hacha (2017) on the performance of RC beams strengthened with Shape Memory Alloy bars of 650 cycles (-34˚C to +34˚C) with a frequency of 3 cycles per day (completed in seven months) are equivalent to much more than 20 years of real life freeze-thaw exposure. The study by Abdelrahman (2011), simulated accumulated 6 and 11 years of freeze-thaw exposure for CFRP wrapped concrete columns in comparison with 252 and 446 cycles, respectively.

In the study by Abdelrahman (2011), investigating the effect of freeze-thaw exposure on the performance of concrete columns wrapped with CFRP sheet, the variation between the set point temperatures inside the environmental chamber and the actual temperature measured by the temperature sensor and the thermocouples embedded inside the concrete columns showed that the temperature readings from the thermocouples inside the concrete column indicate that the maximum and minimum recorded temperatures are close to +20˚C and -18˚C, respectively. The CAN/CSA S6-14 (2014) does not specify any limit to the temperature reached inside the concrete core. Nevertheless, based on ASTM C666/C66M–17, the specified maximum and minimum temperature inside the concrete core during the freeze-thaw cycles were -18˚C and +4.4˚C, respectively. Based on the temperature reading from the thermocouples in the concrete core of the tested columns in the study by Abdelrahman (2011), the temperature limits specified by the ASTM C666/C666M–17 were satisfied.

5 PERFORMANCE EVALUATION AND TESTING

5.1 General

In this research project, Stantec Consulting Ltd. (Stantec) represented the initiator of the idea and cooperated with the University of Calgary (University) who provided the research facility and technical support. The actual testing and evaluation of the durability performance has been carried out at the technical laboratory at the faculty of Civil engineering at the University. One of the key contributions of the facility at the University was the ability to utilize the state-of-the-art climate chamber allowing us to generate severe environmental exposure simulating real weather conditions in accelerated regimes.

5.2 Methodology

The following are the main methodological steps:

1) Design of the beams;
2) Assembly of reinforcement cages;
3) Design and preparation of concrete mix;
4) Casting of the beams;
5) Curing;
6) Pre-cracking the beams, i.e., loading up to 40% of their ultimate flexural capacity in four-point bending;
7) Application of sustained static load to beams placed inside and outside of the climate chamber (sustained load applied throughout entire duration of environmental exposure);
8) Exposure of the loaded beams to defined severe weather conditions in the climate chamber (cycles of freezing and thawing combined with spraying of water-chloride solutions);
9) Acclimatization to ambient temperature and humidity
10) Testing all beams for ultimate flexural capacity in four-point bending; and
11) Data post processing.

The beams were designed according to the Canadian Highway Bridge Design Code (CHBDC), CAN/CSA S6-14 to achieve similar flexural capacity at ultimate loads. From the large number of possible parameters affecting durability testing, the design of the beams, reflecting number of bars and their layout, focused mainly on performance under ultimate flexural loads. While for example crack width at service loads plays an important role, it did not govern the design.

In total, 28 beams were casted to accommodate seven types of rebars, i.e., four beams of each kind. Three beams of each kind were placed in the climate chamber and one beam was left outside as a control beam. The beams representing a bridge parapet were scaled in size, the overall beams dimensions were: length 2000 mm, width 150 mm, and height 300 mm. The supports were spaced 100 mm from each end of the beam giving clear a span of supports of 1800 mm. The beams were designed to result in flexural failure, which was achieved with selected reinforcing ratio of the longitudinal bars less than 2%.

5.3 Materials

The advanced bars were placed at the bottom of the beams, i.e., acting only in tension. Top and shear reinforcement bars comprised conventional black Steel. Each beam consisted of four bars placed in two

layers. While diameter of the bars varied among the beams with different types of bars, it remained the same within a single beam. A typical section of a beam showing the rebar layout is captured in Figure 1.

In the experiment, seven types of internal reinforcing bars were used: 1) conventional black steel by Harris Rebar (BS), 2) stainless steel (SS) by Harris Rebar, 3) Martensitic Micro-composite Formable Steel (MM) by MMFX Technologies-a CMC Company, 4) glass-fibre-reinforced polymers by Hughes Brothers (GF-H), 5) glass-fibre-reinforced polymers by Pultral (GF-P), 6) carbon-fibre-reinforced polymers by Pultral (CF-P), and 7) basalt-fibre-reinforced polymers by Shanghai Shen Xiang CO, Ltd. (BF). Properties of the reinforcing bars are listed in Table 1.

The concrete mix was designed and prepared at the research laboratory of the University to meet requirements of Section 941 – Precast reinforced concrete barriers, Subsection 941.02 – Concrete Quality, of the British Columbia Ministry of Transportation and Infrastructure (BC MoTI). The cementitious components of the concrete comprised 9.9% and 90.2% of fly ash and cement by mass, respectively. The required concrete properties are presented in Table 2. It should be noted that while the minimum requirements were met, variability in specific concrete strength, fc', was greater than expected since the concrete batches were prepared in small volumes individually-reflecting size limitation of the laboratory. Variation of the fc' was also affected by the exposure regimes. Due to high temperatures of the thawing cycle, the fc' of the exposed beams was greater than fc' of the control beams, the difference in fc' ranged between 2 to 14 MPa. Such variation was considered, and collected results were normalized to allow for an accurate evaluation.

5.4 Loading

Both the loading at service and ultimate level was carried out at a four-point testing apparatus. To account for repeatability, permanency, and deviation from non-linearity of the beams, the testing followed ACI 437 R protocol. The setup of the flexural testing apparatus with an actuator of 500 kN capacity is shown in Figure 2. To capture strain distribution in the concrete, three Linear Strain Conversion (LSC) measuring units were installed along vertical sides of the test specimens. To simulate service loads during the exposure, all the beams (including control beams left outside of the climate chamber) were loaded by sustained loads reaching 40% of the calculated flexural capacity. The configuration of the sustained loads applied on the control beams, and beams placed in the climate chamber, is show in Figure 3.

5.5 Simulated Environmental exposure

The environmental exposure was simulated in in a climate chamber allowing for cycles of freezing and thawing in a temperature range between -34°C and +34°C, combined with spraying saltwater with 3.5% NaCl concentration. With frequency of three (3) freeze/thaw cycles per day, in total 195 cycles were completed in 65 days (9.3 weeks ~ 2.3 months). Such accelerated exposure represented an equivalent of 5 years in real conditions. The regimes were selected based on CAN/CSA-S6-14 Figures A3.1.1 and A3.1.2. Diagrams of the defined exposure regimes are shown in Figure 4. Beams exposed in the climate chamber to the spray of chloride-rich solution are shown in Figure 5.

6 RESULTS AND DISCUSSION

6.1 Cracking at service loads

Cracks occurring during service of a reinforced concrete structure play an important role. Cracks represent spots for water and chemical-rich solution to enter the structural member and its reinforcement. During service of a structure, cracks are formed over time upon applied loads and the process of curing concrete such creep and shrinkage. In the case of this study, cracks were generated with the same testing apparatus as used for testing of ultimate flexural capacity, the four-point bending apparatus. The beams were loaded up to 40% of their theoretical flexural capacity. The cracks were generated before exposure in the climate chamber.

The parameters of focus were the crack depth, measured from bottom of the beam to the tip of a crack, and frequency of cracks along the beam. A comparison of these parameters is shown in Figure 6. The figure shows that the modulus elasticity, E, and yield strength, fy, of the bars govern the crack depth as expected. Beams with BF bars (the smallest E) experienced the deepest cracks, ~ 250 mm. On the other hand, beams with MM (the largest E and fy) showed the shallowest cracks, ~ 120 mm. Average depth of cracks in beams with reference black steel reached up to ~140 mm.

From Figure 6 and reviewing the actual cracking patters, a trend can be noted showing that in general beams reinforced with non-metal-based bars experience deeper cracks; however, the depth of the cracks is somewhat uniform along entire length of the beams. Whereas in beams with metal-based bars, the deep cracks form mainly in vicinity of mid-span of the beams.

A comparison of the average number of cracks in beams reinforced with advanced bars to beams with the reference black bars is shown in Figure 7. This comparison shows that the smallest number of cracks occur in beams with BS, closely followed with MM, CF, and GF-P, where the difference is less than 10%. In beams with SS and BF, the average number of cracks is 28% greater than in beams with BS.

From this comparison it can be concluded that number of parameters play a role. It is not only the modulus of elasticity, but also the yield strength and load-strain character of the bar. Also, it is important to realize that while the cracks are deeper in certain beams, it represents a concern to the bars only if those are made of corrosion sensitive materials. In the case of this experiment, top and shear reinforcement comprised corrosion sensitive materials. Nevertheless, durability of concrete may be affected simply by the presence of cracks because with a greater number of deep cracks being present, the risk of more water and chemical-rich solutions entering the structural component becomes higher, which may cause the concrete to deteriorate relatively more rapidly.

6.2 Cracking at ultimate loads

To evaluate the character of cracking patters at ultimate loads, the width of a crack was selected as the main parameter. All cracks on a beam were tracked down during testing for ultimate flexural capacity. A characteristic crack in close vicinity of beam's mid-span was determined and its width monitored. Crack width at maximum load was measured in both the control and exposed beams. Cracks at ultimate were being observed after the exposure in climate chamber.

A comparison of crack width is shown in Figure 8. At a general level, it is apparent that narrower cracks occur in beams with metal-based bars. However, some beams with GH-P and CF experience crack width

smaller than the beams with reference BS, considering the load/capacity ratio. The narrowest cracks are present in beams with MM, measured at 0.2 mm. The widest cracks occur in beams with BF, 2.0 mm.

A comparison of the crack width in exposed beams focusing on the difference between beams with reference BS and advanced bars is shown in Figure 9. The figure shows that beams with metal-based bears experience narrower cracks than beams with BS. Beams with SS represent reduction by 17% and beams with MM by 22%. As expected, beams with non-metal-based bars showed wider cracks than beams with BS, ranging from an increase of 1% (CF-P) to 44% (BF). Such behavior was attributed to the effect of modulus of elasticity and strain of the bars.

The comparison of the crack width at ultimate loads confirmed that it is the modulus of elasticity and quality of concrete that affect overall durability of the structural member, considering its purpose and level of exposure. Similarly, to cracks at service levels, beams with metal-based bars experience relatively narrower cracks. The effect of environmental exposure negatively affected the width of the cracks, mainly enhancing strength of concrete, and therefore, resulting in wider cracks.

6.3 Failure modes and ultimate flexural capacity

Structural behavior reflecting the bar selection and given exposure regime can be described via the ultimate load carrying capacity, maximum achieved displacement, and resulting failure modes.

It should be noted that considering the two main groups of materials, the beams were designed to achieve failure mode by steel yielding (SY) before crushing concrete in metal-based bars and by crushing concrete (CC) before rupture of bars in non-metal-based bars. A comparison of the resulting failure modes, ultimate loads, and relevant deflections is shown in Figure 10. From the figure is apparent that all the beams achieved failure mode as expected, except two beams with MM. These beams experienced both failure modes, affected predominantly by high yield strength of the MM bars. Nevertheless, further investigation showed that it was also the concrete strength, enhanced during the exposure regimes, that contributed to the dual failure modes in beams with MM.

Figure 10 also confirms the trends observed earlier, i.e., modulus of elasticity and stiffness of the bars affect the resulting ultimate load and relevant deflection the most. Beams with BF (smallest E) result in maximum load similar to beams with refence BS (difference ~ 2.5%); however, the relevant displacement increases (difference ~ 60%). In beams with MM, the displacement is close to beams with reference BS (difference ~ 5%). However, the maximum load achieved in beams with MM is significantly greater than in beams with BS (difference ~ 45%). Such behavior was attributed to f_y of the MM bars, which is significantly higher (690 MPa) than in BS (454 MPa) and SS bars (517 MPa).

Failure modes are important to characterize at ultimate loading. During the design phase, a designer needs to be aware of all parameters, including contribution of the bars, that can influence resulting failure mode. It is the strength of the bar in combination with strength of concrete that control the resulting failure mode, affecting mainly the safety during service-avoiding unexpected failures. Nevertheless, the significance of the environmental exposure on this parameter has not been found.

To normalize the ultimate flexural capacity of all the beams (dependent of number of factors), it was determined that the main parameter will be the flexural stiffness at ultimate. Flexural stiffness at ultimate encompasses factors such as crack distribution, strength of bars, strength of concrete, as well as environmental exposure.

The effect of exposure on flexural capacity, via flexural stiffness, is shown in Figure 11. As identified earlier, strength of the bars and modulus of elasticity play the paramount role. Beams with MM achieve the greatest stiffness, and beams with BF the lowest as expected. However, another parameter occurred to play a role, the strain at ultimate. While beams with BF experienced the smallest stiffness, their modulus of elasticity (53 GPa) is greater than GF-H bars (46 GPa). However, the strain at ultimate of GF-H (1.4%) is smaller than in BF (2.0%).

Figure 11 also indicates the difference between stiffness of the exposed and control beams. In other words, it shows how the exposure affects the flexural stiffness. Knowing that the exposure regimes improve the strength of the concrete, it can be derived that the durability of the member will dictate the level of concrete strength improvement. In other words, the beams with overall low durability (experiencing a lot of concrete spalling, cracks, etc.) will result in low improvement of flexural stiffness. These assumptions indicate that, when considering solely ultimate flexural capacity, the beams with SS and MM experience the smallest impact of the exposure. The difference between control and exposed beams is high in beams with SS: 84% and MM: 89%. On the other hand, beams BF experience difference between the control and exposed beams only 3%, indicating high influence of the exposure.

The exposure regime affects the overall durability of the member. Considering the ultimate flexural capacity as the main objective, it can be concluded that members reinforced with metal-based bars are affected by the exposure regime not as significantly as members with non-metals-based bars. It was the concrete that was affected by the environmental exposure the most. However, based on the observations, it can be said that the conditions of the concrete were influenced also by performance of the reinforcing bars.

6.4 Load-deflection relationship

Load-deflection relationship is a valuable tool to identify characteristics of the applied materials in specific assemblies. The load-deflection relationship of the control and exposed beams is shown in Figure 12. From the figure, it is apparent that a similar trend occurred at the pre-cracking stage, i.e., the linear portion of the diagram (loads up to 40% of calculated maxima). However, upon reaching this level, a more significant difference occurred in the response. It is the modulus elasticity of the bars that controlled the response. This attribute is clearly apparent in the exposed beams. However, from further observation it can be concluded that the effect of exposure had only minimal impacts on the character of the load-deflection relationship of beams tested herein.

6.5 Ductility

Ductility of reinforced concrete structures is an important parameter as it represents the ability of a member to sustain significant deformations while keeping its resistance. Such behavior is highly desirable as it provides sufficient warning in cases of overloading and also in seismically active regions.

To overcome the lack of yielding plateau in the group of non-metal-based bars, ductility of all beams was evaluated via deformability index. This index is calculated as a ratio of energy dissipated at ultimate loads over energy dissipated at service loads. The dissipated energy is calculated as the area under the load-deflection curve. Deformability index of the exposed beams is show in Figure 13. From the figure is apparent that beams reinforced with SS experience the greatest ductility as expected. Beams with MM resulted in slightly lower ductility (4%) than beams with SS, reflecting smaller strains at ultimate. The group of beams reinforced with non-metal-rebars remained within similar range. As expected, these

beams resulted in deformability index 28% smaller than beams with metal-based bars. Beams with GF-P achieved the greatest deformability index among the non-metal-based bars. Deformability index of beams with GF-H and CF-P is 7% smaller than GF-P. The beams with BF reported deformability index 15% smaller than beams with GF-P, indicating the smallest ductility.

The evaluation disclosed that the influence of the applied exposure regimes on ductility of the beams was marginal. It can be concluded that in applications where ductility of members may play a significant role, metal-based bars represent a more suitable choice.

7 CONCLUSIONS

It can be said that the experimental testing of the durability performance disclosed several new findings and confirmed an expected behavior in some areas. The effect of seven different bar types was evaluated in five categories covering the majority of structural performance categories for a typical bridge parapet exposed to harsh environmental conditions. When considering the main objective, the flexural capacity and structural behavior up to ultimate, it can be concluded that properties such as modulus of elasticity of all bars and yield strength of metal-based bars played the most significant role. The accelerated environmental exposure affected mainly performance and deterioration of the concrete. Nevertheless, performance of the concrete in return reflected the performance of the various bars. Flexural capacity and behavior of the beams were affected by the exposure most significantly. On the other hand, the character of cracking patterns and ductility were influenced only at marginal levels.

Results and conclusions of the research are summarized in a matrix shown in Table 3. This table can be used by designers, engineers, and/or asset managers as a guideline when considering applications dominantly utilizing flexural performance of the infrastructure assemblies such as bridges, parking garages, retaining walls, building foundations, and/or marine structures. The table shows the achieved level of improved specific performance category when an advanced type of bar is selected over the conventional black bar.

8 REFERENCE

Abdelrahman, K. 2011, “Effectiveness of Steel Fibre Reinforced Polymer Sheets for Confining Circular Concrete Columns”. MSc Thesis. University of Calgary. Canada.

Bisby, L., Green, M. 2002. "Resistance to Freezing and Thawing of Fiber-Reinforced Polymer-Concrete Bond". ACI Structural Journal. 99 (2). pp. 215-223.

Chen, Y., Davalos, J. F., Ray, I., Kim, H. 2007. “Accelerated aging tests for evaluations of durability performance of FRP reinforcing bars for concrete structures”. Composite Structures. Volume 78. Issue 1. March 2007. pp. 101–111.

Davalos, J. F., Chen, Y., Ray, I. 2008. “Effect of FRP bar degradation on interface bond with high strength concrete”. Cement and Concrete Composites. Volume 30. Issue 8. September 2008. pp. 722–730.

DeJong, J. S., Heffernan, P. J., MacDougall, J. 2009. “Periodic Overload Corrosion Fatigue of MMFX and Stainless Reinforcing Steels”. Journal of Materials in Civil Engineering. Volume 21 Issue 1 - January 2009. pp. 278-290.

Fraser, J. K. 1959. “Freeze-thaw frequencies and mechanical weathering in Canada.” Arctic. 12(1). pp. 40-53.

Ho, E., Gough, A. W. 2005. "Freeze thaw cycles in Toronto, Canada in a changing climate". Theoretical and Applied Climatology, 83 (1). pp. 203-210.

Rojob, H., El-Hacha, R., 2017. “Self-prestressing using Iron-based Shape Memory Alloy for Flexural Strengthening of Reinforced Concrete Beams”. American Concrete Institute (ACI). Volume: 114, Issue Number: 2. March 2017. pp. 523-532.

Kahl, S., 2007. “Corrosion resistant alloy steel (MMFX) reinforcing bar in bridge decks”. Michigan DOT. construction and technology division. Report No.: R-1499.

Laoubi, K., El-Salakawy, E., Benmokrane, B. 2006. “Creep and durability of sand-coated glass FRP bars in concrete elements under freeze/thaw cycling and sustained loads”. Cement & Concrete Composites. 28(10): 869-878.

Lu, Z., Xian, G., Li, H. 2015. “Effects of elevated temperatures on the mechanical properties of basalt fibers and BFRP plates”. Construction and Building Materials. Volume 127. 30 November 2016. pp. 1029–1036.

Micelli, F., Nanni, A. 2004. “Durability of FRP rods for concrete structures. Construction and Building Materials”, Volume 18. Issue 7. September 2004. pp. 491–503.

Omran, H.Y., 2013, “Long-Term Flexural Performance of Prestressed-NSM-CFRP Strengthened RC Beams”. PhD Thesis. University of Calgary. Canada.

Omran, H. Y., El-Hacha, R. 2014. "Effects of Sustained Load and Freeze-Thaw Exposure on RC Beams Strengthened with Prestressed NSM-CFRP Strips". Advances in Structural Engineering. 17 (12). pp. 1801-1816.

Ormelese, M., Bolzoni, F., Perez, E.R., Goidanich, S. 2007. “Migrating corrosion inhibitors for reinforced concrete structures”. NACE International. CORROSION 2007. 11-15 March. Nashville. Tennessee. pp 79-83.

Polder, R., Leegwater, G., Worm, D., Courage, W., 2014. “Service life and life cycle cost modelling of cathodic protection systems for concrete structures”. Cement and Concrete Composites. Volume 47. March 2014, pp. 69–74.

Quagliarini, E., Monni, F., Bondioli, F., Lenci, S. 2016. “Basalt fiber ropes and rods: Durability tests for their use in building engineering”. Journal of Building Engineering. Volume 5. March 2016. pp. 142–150.

Shao, Y., Jia, C., Meng, G., Zhang, T. 2009. “The role of a zinc phosphate pigment in the corrosion of scratched epoxy-coated steel”. Corrosion Science, Volume 51, Issue 2, February 2009, pp. 371–379.

ASTM C666 / C66M – 15. 2015. “Standard Test Method for Resistance of Concrete to Rapid Freezing and Thawing”

437.1R-07. Load Tests of Concrete Structures: Methods, Magnitude, Protocols & Acceptance Criteria.

ASTM A706 / A706M-16. “Standard Specification for Deformed and Plain Low-Alloy Steel Bars for Concrete Reinforcement”.

ASTM A955/A955M-14. “Standard Specification For Deformed And Plain Stainless-Steel Bars For Concrete Reinforcement”.

ASTM A1035/A1035M-09. “Specification “Deformed and Plain, Low-carbon, Chromium, Steel Bars for Concrete Reinforcement”.

CAN/CSA-S6-14. 2014 "CSA S6-14 (Canadian Highway Bridge Design Code)". Mississauga. Ontario: Canadian Standard Association.

Standard Specifications for Highway Construction VOL 2/2, Section 941 Precast reinforced concrete barriers. British Columbia – Ministry of Transportation and Infrastructure, 2016.

9 TABLES

Table 1 – Properties of the reinforcing bars

Rebar	Grade	E [GPa]	Diam. [mm]	$As_{(TOT)}$ [mm^2]	fy [MPa]	fu [MPa]	Strain*
BS	Grade 400W	200	15.9	796	454	618	14.0%
SS	Grade 500 (Duplex Alloy)	200	15.9	796	517	689	20.0%
MM	ChrōmX 9100. Grade 100	200	15.9	796	690	1030	7.0%
GF-H	Aslan 100	46	22.0	1548	N/A	655	1.4%
GF-P	V-Rod Grade 60	60	19.1	1136	N/A	1100	2.1%
CF-P	V-Rod Carbon	144	13.0	507	N/A	1765	1.3%
BF	Grade 52	52	19.0	1136	N/A	1050	2.0%

LEGEND: E – Modulus of elasticity; $As_{(TOT)}$ – Total area of reinforcing bars within a beam; fy – Yield strength; fu – Ultimate strength; * Minimum as per relevant ASTM standard

Table 2: Concrete properties

Item	Required Property
Compressive strength	30 MPa
Minimum cement content	320 kg/m^3
Maximum water/cement ratio	0.45
Coarse aggregate maximum size	28 mm
Slump	50 mm ± 20 mm
Entrained air	5 to 8%.

Table 3: Matrix indicating the improved level of performance in comparison to black steel

Parameter	Advanced Material					
	SS	MM	GF-H	GF-P	CF-P	BF
Cracking up to 40%	●●	●●●●	●●●	●●●	●●●	●●
Cracking up to 100%	●●●●	●●●●●	●●	●●	●●●	●
Flexural capacity	●●●●	●●●●●	●●	●●●●	●●	●
Load-deflection resp.	●●●●	●●●●●	●●	●●●	●●	●
Ductility	●●●●●	●●●●●	●●●	●●●	●●●	●●●

Improvement: *High:* ●●●●● *Medium-High:* ●●●● *Medium* ●●● *Low-Medium:* ●● *Low:* ●

10 FIGURES

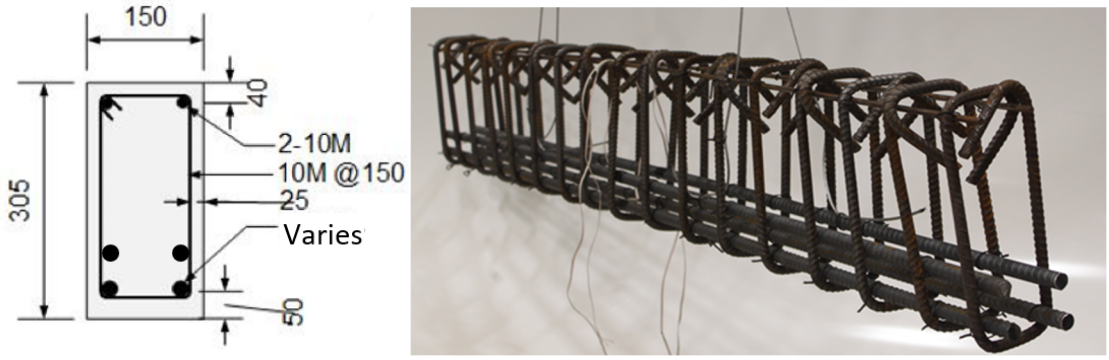

Figure 1: Typical cross-section of a test specimen and a rebar cage before placement into a casting form

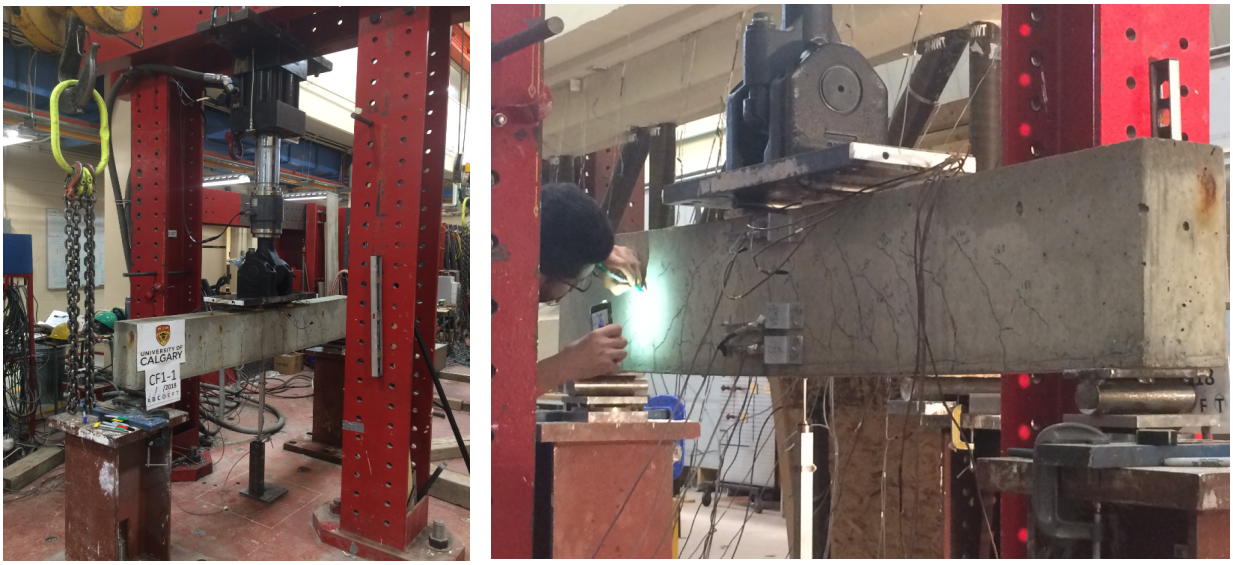

Figure 2: Four-point flexure testing apparatus

Figure 3: Sustained load applied on control beams and beams placed in the climate chamber

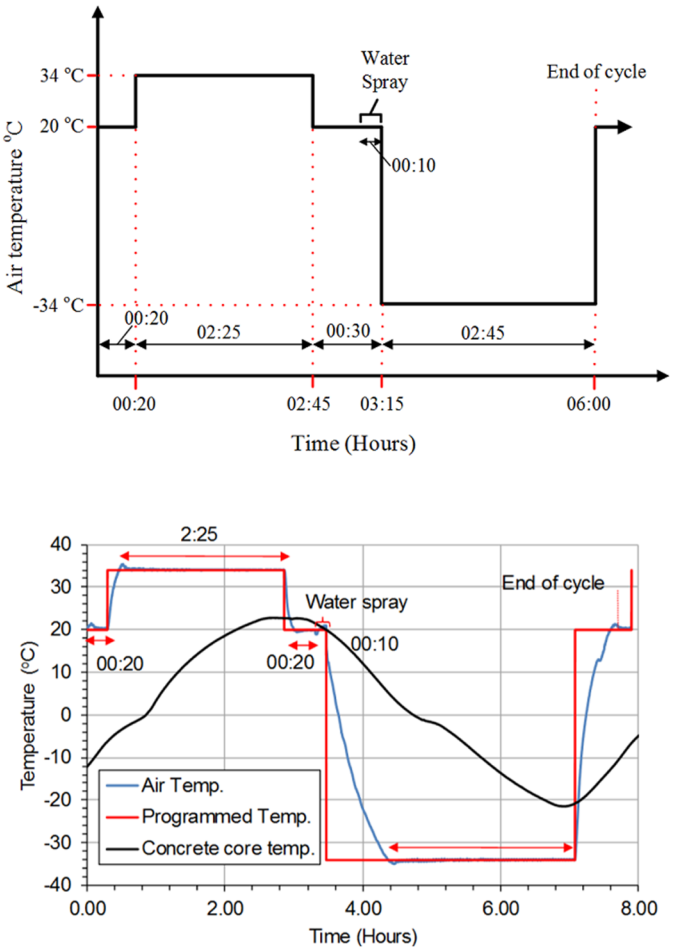

Figure 4: Exposure regimes in the climate chamber simulating real life conditions

Figure 5: Spraying of chloride rich solution in the climate chamber

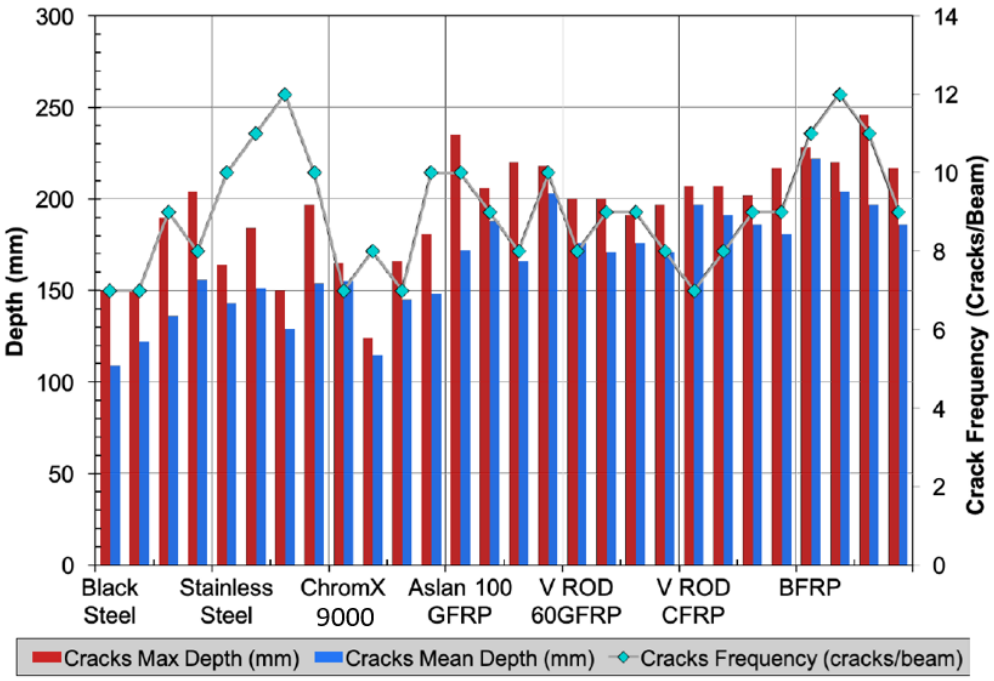

Figure 6: Crack depth and frequency of cracks in beams at service loads before exposure

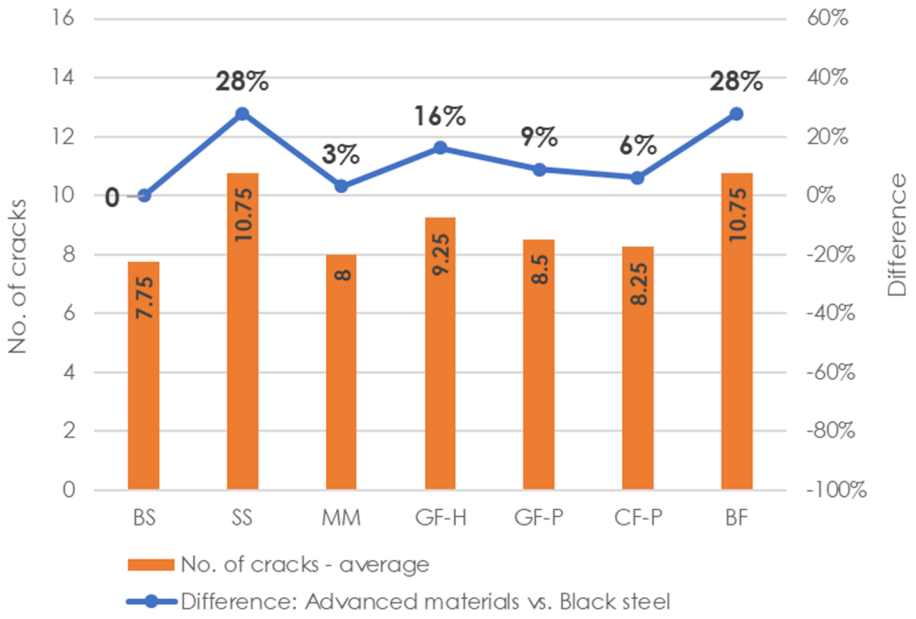

Figure 7: A comparison of the average number of cracks in beams with advanced bars and reference black bars

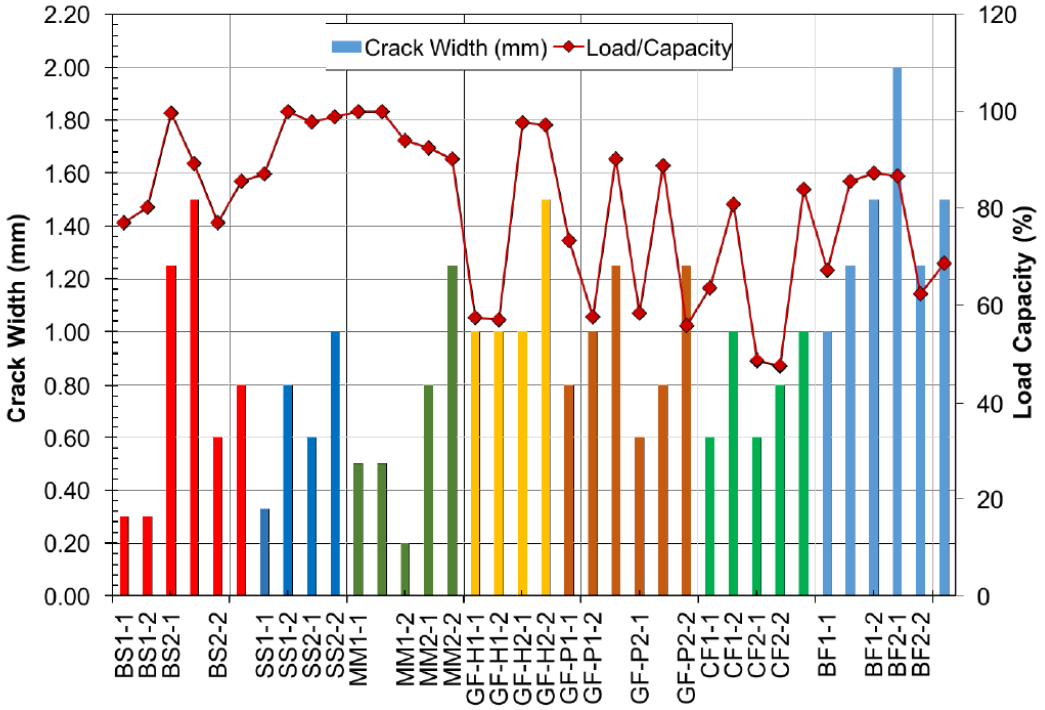

Figure 8: Crack width and relevant load in control and exposed beams

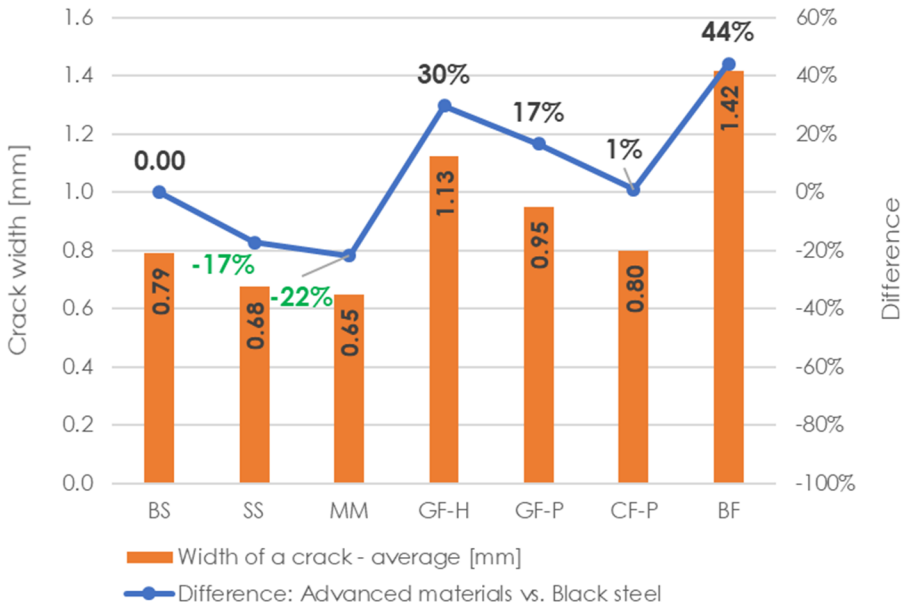

Figure 9: Comparison of crack width at ultimate loads in the exposed beams

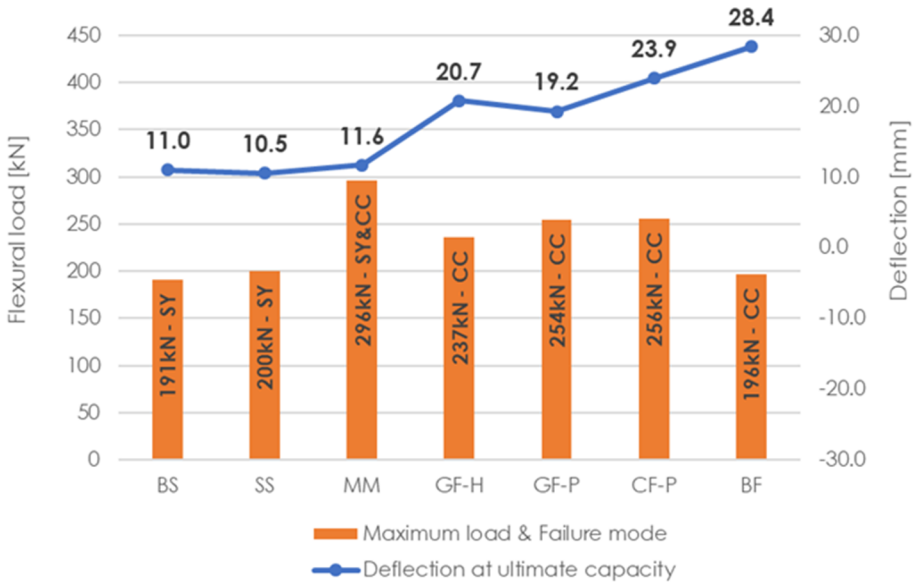

Figure 10: Failure modes at ultimate loads with relevant deflections in exposed beams

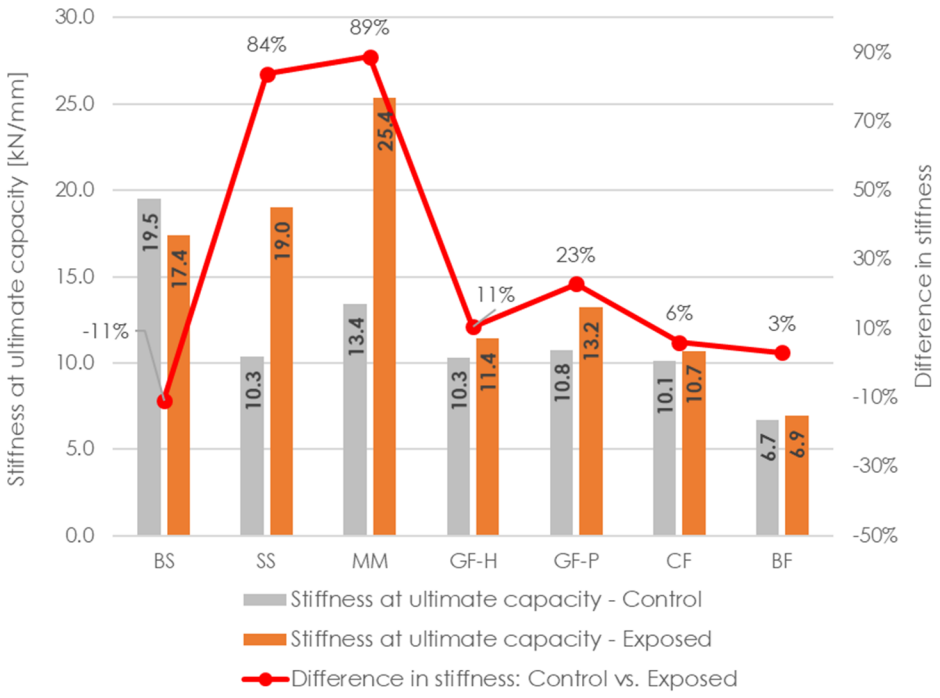

Figure 11: Effect of exposure on flexural capacity

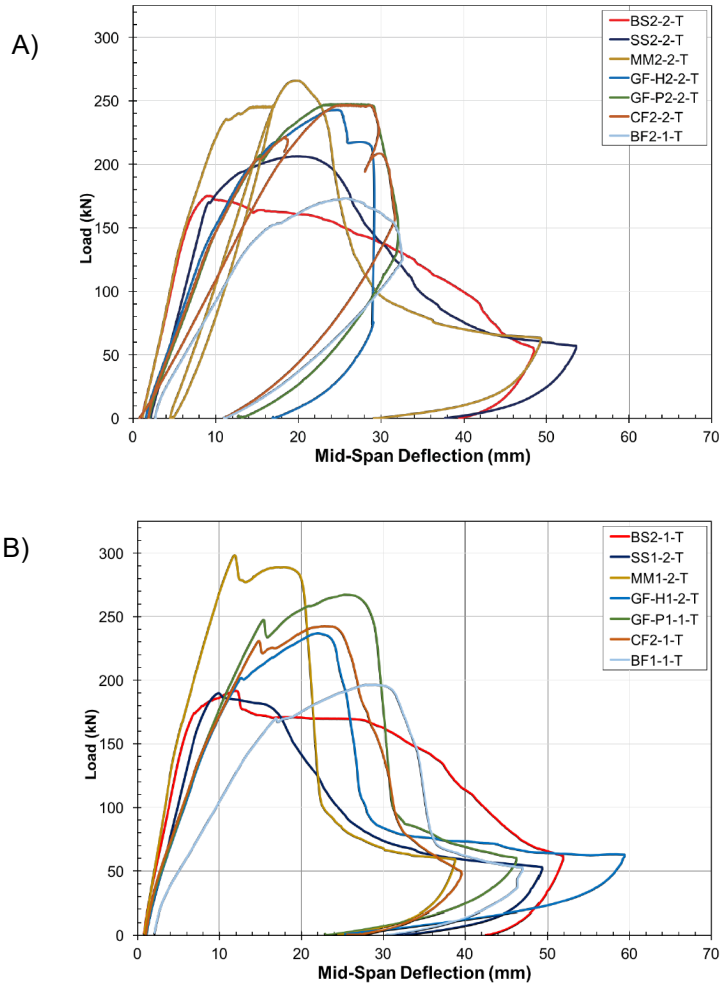

Figure 12: Load-deflection relationship: A) Control beams, B) Exposed beams

Figure 13: Ductility index of the exposed beams